Structural Engineering and Mechanics, *Vol. 71, No. 2 (2019) 153-163*
DOI: https://doi.org/10.12989/sem.2019.71.2.153

Longitudinal cracks in non-linear elastic beams exhibiting material inhomogeneity

Victor I. Rizov*

Department of Technical Mechanics, University of Architecture, Civil Engineering and Geodesy, 1 Chr. Smirnensky blvd., 1046, Sofia, Bulgaria

(Received September 3, 2018, Revised March 26, 2019, Accepted March 27, 2019)

Abstract. Longitudinal fracture behavior of non-linear elastic beam configurations is studied in terms of the strain energy release rate. It is assumed that the beams exhibit continuous material inhomogeneity along the width as well as along the height of the cross-section. The Ramberg-Osgood stress-strain relation is used for describing the non-linear mechanical behavior of the inhomogeneous material. A solution to strain energy release rate is derived that holds for inhomogeneous beams of arbitrary cross-section under combination of axial force and bending moments. Besides, the solution may be applied at any law of continuous distribution of the modulus of elasticity in the beam cross-section. The longitudinal crack may be located arbitrary along the beam height. The solution is used to investigate a longitudinal crack in a beam configuration of rectangular cross-section under four-point bending. The crack is located symmetrically with respect to the beam mid-span. It is assumed that the modulus of elasticity varies continuously according a cosine law in the beam cross-section. The longitudinal fracture behavior of the inhomogeneous beam is studied also by applying the J-integral approach for verification of the non-linear solution to the strain energy release rate derived in the present paper. Effects of material inhomogeneity, crack location along the beam height and non-linear mechanical behavior of the material on the longitudinal fracture behavior are evaluated. Thus, the solution derived in the present paper can be used in engineering design of inhomogeneous non-linear elastic structural members to assess the influence of various material and geometrical parameters on longitudinal fracture.

Keywords: inhomogeneous beam; longitudinal fracture; material nonlinearity; strain energy

1. Introduction

Since the properties of inhomogeneous materials vary from place to place in the volume of the body, the investigation of fracture behavior of inhomogeneous structural members and components is more laborious. Typical examples for inhomogeneous materials are the functionally graded materials. Due to the gradual variation in the composition along one or more spatial coordinates, the properties of functionally graded materials can be optimized so as to achieve high performance and material efficiency (Koizumi 1993, Markworth, Ramesh and Parks 1995, Mortensen and Suresh 1995, Neubrand and Rödel 1997, Suresh and Mortensen 1998, Hirai and Chen 1999, Gasik 2010, Nemat-Allal *et al.* 2011, Bohidar, Sharma and Mishra 2014). Also, the gradation in material properties leads to significant reduction of thermal stresses, residual stresses, and stress concentration. Thus, it is not surprising that the application of the functionally graded materials in complex and sophisticated components which cannot be made of the conventional metal structural materials in aeronautics, nuclear reactors, turbine rotors, electronics and biomedicine has been gradually increasing for the last decades.

The appropriate application of inhomogeneous materials demands an adequate understanding of their mechanical properties, and fracture behavior and characteristics. The longitudinal fracture behavior of inhomogeneous structural members and components is particularly important since certain kinds of inhomogeneous materials, such as functionally graded materials, can be built up layer by layer (Bohidar, Sharma and Mishra 2014) which is a premise for appearance of longitudinal cracks between layers. In view of the complex character of longitudinal fracture of inhomogeneous materials and structures, the development of analyses of this fracture phenomenon is of great importance. Fracture analyses are very useful for studying the effects of various factors such as crack location, material inhomogeneity and the non-linear mechanical behavior of the material on the longitudinal fracture. The information gathered through these analyses can be used to develop and improve inhomogeneous materials with respect to their longitudinal fracture performance. Thus, it is not surprising that fracture in inhomogeneous (functionally graded) structural members and components remains a topic of active research around the globe (Wang and Noda 2001, Carpinteri, Paggi and Pugno 2006, Dong Wei, Yinghua Liu and Zhihai Xiang 2012, Mousavi and Paavola 2013, Rekik, El-Borgi and Ounaies 2014).

Fracture behavior of functionally graded composite structures under thermal loading has been studied and discussed in detail by Wang and Noda (2001). Linear-elastic behavior of the functionally graded material has been assumed in fracture analysis. Different crack positions and material gradients have been investigated in a functionally graded material bonded to a metal substrate.

*Corresponding author, Professor
E-mail: v_rizov_fhe@uacg.bg

http://www.techno-press.com/journals/sem&subpage=7
ISSN: 1225-4568 (Print), 1598-6217 (Online)

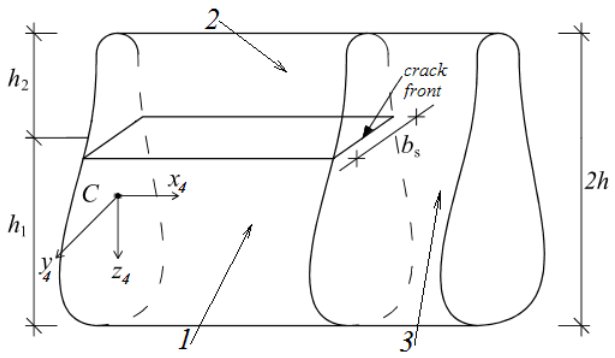

Fig. 1 Beam portion with the crack front (1 – lower crack arm, 2 – upper crack arm and 3 – un-cracked part of the beam). The heights of the lower and upper crack arms are denoted by h_1 and h_2, respectively.

An approach for studying of brittle cracking in functionally graded materials has been developed by Carpinteri, Paggi and Pugno (2006). The approach can also be applied for fatigue fracture behavior. The methods of linear-elastic fracture mechanics have been applied. A detailed study of fracture in a three-point bending functionally graded beam configuration with an edge crack has been carried-out. An edge crack in a functionally graded plate loaded in tension has been addressed too. The problem of fracture behavior of a two-layer beam with an external functionally graded layer subjected to three-point bending has also been analyzed.

Edge cracks in functionally graded linear-elastic beams with axial loading have been investigated by Dong Wei, Yinghua Liu and Zhihai Xiang (2012). The rotational spring model has been used in order to treat the discontinuity caused by the crack. The governing equations of motion have been established and solved. Beams with an arbitrary number of edge cracks have been analyzed. The influences of loading conditions, location and number of cracks and end supports have been discussed.

A cracked functionally graded piezoelectric-piezomagnetic layer has been investigated by Mousavi and Paavola (2013). Problems of arbitrary configurations of multiple embedded and edge cracks have been considered. Straight and curved cracks have been analyzed.

The problem of an axisymmetric penny shaped crack embedded in functionally graded magneto electro elastic medium has been addressed by Rekik, El-Borgi and Ounaies (2014). It has been assumed that the linear-elastic material is functionally graded in axisymmetric direction. The effect of material non-homogeneity and varying crack geometry has been investigated.

Several works concentrated on longitudinal fracture behavior of inhomogeneous non-linear elastic beam structures loaded in bending have been published recently by the author (Rizov 2017a, b, c, d, Rizov 2018a, b, c). Particular solutions to the strain energy release rate for longitudinal cracks in separate beam configurations of rectangular cross-section have been derived (Rizov 2017a, b, c, d, Rizov 2018a, b, c).

The present paper is focused on analysis of longitudinal fracture of inhomogeneous beam structures of arbitrary cross-section by using the Ramberg-Osgood stress-strain relation for modeling the non-linear mechanical behavior of the material. The beams considered are under combination of axial force and bending moments. Besides, it is assumed that the beams exhibit smooth material inhomogeneity along the width as well as along the height. The main purpose of the present paper is to derive a general solution to the strain energy release rate assuming that the modulus of elasticity varies continuously in both width and height directions of the beam cross-section. It should be mentioned that the solution holds for monotonic loading, small strains (first order), prismatic beams (Euler-Bernoulli assumption) under the exclusion of body forces.

The solution is verified by the *J*-integral approach. Finite element simulations are also performed to verify the solution.

2. Theoretical formulation

A beam portion with the crack front is shown in Fig. 1. The longitudinal crack is located arbitrary along the beam height. The heights of the lower and upper crack arms are h_1 and h_2, respectively. By applying the approach developed in (Rizov 2017b), the strain energy release rate, G, for the inhomogeneous beam in Fig. 1 can be expressed as

$$G = \frac{1}{b_S}\left(\iint_{(A_1)} u_{01}^{*} dA_1 + \iint_{(A_2)} u_{02}^{*} dA_2 - \iint_{(A_3)} u_{03}^{*} dA_3 \right) \quad (1)$$

where b_s is the beam width at the level of the longitudinal crack, u_{01}^{*}, u_{02}^{*} and u_{03}^{*} are, respectively, the complementary strain energy densities in the cross-sections of lower and upper crack arms behind the crack front and in the beam cross-section ahead of the crack front, A_1, A_2 and A_3 are the areas of cross-sections of the crack arms behind the crack front and the cross-section of the beam ahead of the crack front.

The Ramberg-Osgood stress-strain relation is written as (Dowling 2007)

$$\varepsilon = \frac{\sigma}{E} + \left(\frac{\sigma}{H}\right)^{\frac{1}{n}} \quad (2)$$

where ε is the longitudinal strain, σ is the longitudinal normal stress, E is the modulus of elasticity, H and n are material properties. The first term in the right-hand side of Eq. (2) describes the linear-elastic strains. The non-linear mechanical behavior of the material is described by the second term in the right-hand side of Eq. (2). It should be noted that the uniqueness of stress for a given strain does not hold for the Ramberg-Osgood stress-strain relation under unloading conditions. Thus, considering stress-redistribution effects, unloading might occur during crack propagation. Therefore, the solution to the strain energy release rate derived in the present paper is restricted to crack initiation.

For the Ramberg-Osgood stress-strain relation, the complementary strain energy density in the cross-section of

lower crack arm behind the crack front can be expressed as (Rizov 2018a)

$$u_{01}^{*} = \frac{\sigma^2}{2E} + \frac{n\sigma^{\frac{1+n}{n}}}{(1+n)H^{\frac{1}{n}}} \tag{3}$$

It is obvious that σ cannot be determined explicitly from equation Eq. (2). Therefore, the normal stress in the cross-section of lower crack arm behind the crack front is expanded in series Maclaurin by keeping the first six members

$$\begin{aligned}\sigma(y_1,z_1) \approx \sigma(0,0) + \frac{\partial\sigma(0,0)}{\partial y_1}y_1 + \frac{\partial\sigma(0,0)}{\partial z_1}z_1 + \\ + \frac{\partial^2\sigma(0,0)}{2!\partial y_1^2}y_1^2 + + \frac{\partial^2\sigma(0,0)}{\partial y_1\partial z_1}y_1z_1 + \frac{\partial^2\sigma(0,0)}{2!\partial z_1^2}z_1^2\end{aligned} \tag{4}$$

where y_1 and z_1 are the centroidal axes of the lower crack arm cross-section (Fig. 2). Eq. (4) is re-written as

$$\begin{aligned}\sigma(y_1,z_1) \approx \mu_1 + \mu_2 y_1 + \mu_3 z_1 + \mu_4 y_1^2 + \\ \mu_5 y_1 z_1 + \mu_6 z_1^2\end{aligned} \tag{5}$$

The Ramber-Osgood Eq. (2) is used to determine the coefficients, μ_1, μ_2, μ_3, μ_4, μ_5 and μ_6. By applying the Bernoulli's hypothesis for plane sections, the strains in the lower crack arm cross-section are expressed as

$$\varepsilon = \varepsilon_{C_1} + \kappa_{y_1} y_1 + \kappa_{z_1} z_1 \tag{6}$$

where ε_{C_1} is the strain in the centre of the lower crack arm cross-section, κ_{y_1} and κ_{z_1} are the curvatures of lower crack arm in the x_1y_1 and x_1z_1 planes, respectively. It should be noted that the Bernoulli's hypothesis can be applied since beams of high span to height ratio are under consideration in the present paper. By combining of Eqs. (5), (6) and (2), one arrives at

$$\begin{aligned}\varepsilon_{C_1} + \kappa_{y_1} y_1 + \kappa_{z_1} z_1 = \\ \frac{\mu_1 + \mu_2 y_1 + \mu_3 z_1 + \mu_4 y_1^2 + \mu_5 y_1 z_1 + \mu_6 z_1^2}{E} + \\ + \frac{\left(\mu_1 + \mu_2 y_1 + \mu_3 z_1 + \mu_4 y_1^2 + \mu_5 y_1 z_1 + \mu_6 z_1^2\right)^{\frac{1}{n}}}{H^{\frac{1}{n}}}\end{aligned} \tag{7}$$

where

$$E = E(y_1, z_1) \tag{8}$$

By substituting of $y_1 = 0$ and $z_1 = 0$ in Eq. (7), one obtains

$$\varepsilon_{C_1} = \frac{\mu_1}{E} + \frac{\mu_1^{\frac{1}{n}}}{H^{\frac{1}{n}}} \tag{9}$$

Further, by substituting of $y_1 = 0$ and $z_1 = 0$ in the first derivatives of Eq. (7) with respect to y_1 and z_1, one arrives at

$$\begin{aligned}\kappa_{y_1} E + \varepsilon_{C_1}\frac{\partial E}{\partial y_1} = \mu_2 + \\ + \frac{1}{H^{\frac{1}{n}}}\left(\frac{\partial E}{\partial y_1}\mu_1^{\frac{1}{n}} + E\frac{1}{n}\mu_1^{\frac{1-n}{n}}\mu_2\right)\end{aligned} \tag{10}$$

$$\begin{aligned}\kappa_{z_1} E + \varepsilon_{C_1}\frac{\partial E}{\partial z_1} = \mu_3 + \\ + \frac{1}{H^{\frac{1}{n}}}\left(\frac{\partial E}{\partial z_1}\mu_1^{\frac{1}{n}} + E\frac{1}{n}\mu_1^{\frac{1-n}{n}}\mu_3\right)\end{aligned} \tag{11}$$

Similarly, by substituting of $y_1 = 0$ and $z_1 = 0$ in the second derivatives of Eq. (7) with respect to y_1 and z_1, one obtains

$$\begin{aligned}2\kappa_{y_1}\frac{\partial E}{\partial y_1} + \varepsilon_{C_1}\frac{\partial^2 E}{\partial y_1^2} = 2\mu_4 + \\ + \frac{1}{H^{\frac{1}{n}}}\Bigg[\frac{\partial^2 E}{\partial y_1^2}\mu_1^{\frac{1}{n}} + \frac{\partial E}{\partial y_1}\frac{1}{n}\mu_1^{\frac{1-n}{n}}\mu_2 + \\ + \left(\frac{\partial E}{\partial y_1}\frac{1}{n}\mu_1^{\frac{1-n}{n}} + E\frac{1-n}{n^2}\mu_1^{\frac{1-2n}{n}}\mu_2\right)\mu_2 + E\frac{2}{n}\mu_1^{\frac{1-n}{n}}\mu_4\Bigg]\end{aligned} \tag{12}$$

$$\begin{aligned}\kappa_{y_1}\frac{\partial E}{\partial z_1} + \kappa_{z_1}\frac{\partial E}{\partial y_1} + \varepsilon_{C_1}\frac{\partial^2 E}{\partial y_1\partial z_1} = \mu_5 + \\ + \frac{1}{H^{\frac{1}{n}}}\Bigg[\frac{\partial^2 E}{\partial y_1\partial z_1}\mu_1^{\frac{1}{n}} + \frac{\partial E}{\partial y_1}\frac{1}{n}\mu_1^{\frac{1-n}{n}}\mu_3 + \\ + \left(\frac{\partial E}{\partial z_1}\frac{1}{n}\mu_1^{\frac{1-n}{n}} + E\frac{1-n}{n^2}\mu_1^{\frac{1-2n}{n}}\mu_3\right)\mu_2 + E\frac{1}{n}\mu_1^{\frac{1-n}{n}}\mu_5\Bigg]\end{aligned} \tag{13}$$

$$\begin{aligned}2\kappa_{z_1}\frac{\partial E}{\partial z_1} + \varepsilon_{C_1}\frac{\partial^2 E}{\partial z_1^2} = 2\mu_6 + \\ + \frac{1}{H^{\frac{1}{n}}}\Bigg[\frac{\partial^2 E}{\partial z_1^2}\mu_1^{\frac{1}{n}} + \frac{\partial E}{\partial z_1}\frac{1}{n}\mu_1^{\frac{1-n}{n}}\mu_3 + \\ + \left(\frac{\partial E}{\partial z_1}\frac{1}{n}\mu_1^{\frac{1-n}{n}} + E\frac{1-n}{n^2}\mu_1^{\frac{1-2n}{n}}\mu_3\right)\mu_3 + \\ + E\frac{2}{n}\mu_1^{\frac{1-n}{n}}\mu_6\Bigg]\end{aligned} \tag{14}$$

In Eqs. (9)-(14), E and the derivatives, $\frac{\partial E}{\partial y_1}$, $\frac{\partial E}{\partial z_1}$, $\frac{\partial^2 E}{\partial y_1^2}$, $\frac{\partial^2 E}{\partial y_1\partial z_1}$ and $\frac{\partial^2 E}{\partial z_1^2}$, are calculated at $y_1 = 0$ and $z_1 = 0$.

There are nine unknowns, μ_1, μ_2, μ_3, μ_4, μ_5, μ_6, ε_{c1}, κ_{y1} and κ_{z1}, in Eqs. (9)-(14). Three other equations are

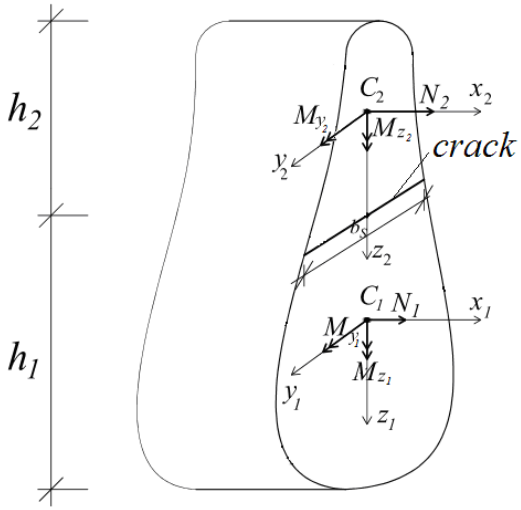

Fig. 2 Geometry and loading of the lower and upper crack arm cross-sections behind the crack front

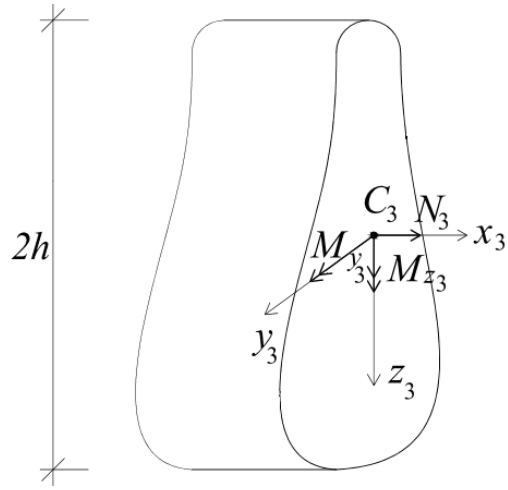

Fig. 3 Geometry and loading of the beam cross-section ahead of the crack front

constructed by considering the equilibrium of the elementary forces in the lower crack arm cross-section. Since the lower crack arm cross-section is under combination of axial force, N_1, and bending moments, M_{y_1} and M_{z_1}, (Fig. 2) the equilibrium equations are written as

$$N_1 = \iint_{(A_1)} \sigma dA_1 \tag{15}$$

$$M_{y_1} = \iint_{(A_1)} \sigma z_1 dA_1 \tag{16}$$

$$M_{z_1} = \iint_{(A_1)} \sigma y_1 dA_1 \tag{17}$$

By using the MatLab computer program, Eqs. (9)-(17) should be solved with respect to μ_1, μ_2, μ_3, μ_4, μ_5, μ_6, ε_{C_1}, κ_{y_1} and κ_{z_1}, for particular beam configuration, loading conditions and material properties. Then, u_{01}^* can be obtained by substituting of Eq. (5) in Eq. (3).

Eq. (3) can also be applied to calculate u_{02}^*. For this purpose, σ has to be replaced with σ_d where σ_d is the normal stress in the cross-section of the upper crack arm behind the crack front. Also, μ_1, μ_2, μ_3, μ_4, μ_5, μ_6, y_1, z_1, N_1, M_{y_1}, M_{z_1}, A_1, ε_{c1}, κ_{y1} and κ_{z1} have to be replaced, respectively, with μ_{d1}, μ_{d2}, μ_{d3}, μ_{d4}, μ_{d5}, μ_{d6}, y_2, z_2, N_2, M_{y_2}, M_{z_2}, A_2, ε_{C_2}, κ_{y_2} and κ_{z_2} in Eqs. (9)-(17). Here, y_2 and z_2 are the centroidal axes of the upper crack arm cross-section, N_2, M_{y_2}, M_{z_2} are the axial force and the bending moments (Fig. 2), ε_{C_2}, κ_{y_2} and κ_{z_2} are the strain in the centre of the upper crack arm cross-section, and the curvatures of upper crack arm in the x_2y_2 and x_2z_2 planes, respectively.

The complementary strain energy density in the beam cross-section ahead of the crack front can be obtained by replacing of σ with σ_f in Eq. (3). Here, σ_f is the normal stress in the beam cross-section ahead of the crack front. Besides, in Eqs. (9)-(17), μ_1, μ_2, μ_3, μ_4, μ_5, μ_6, y_1, z_1, N_1, M_{y_1}, M_{z_1}, A_1, ε_{C_1}, κ_{y_1} and κ_{z_1} have to be replaced with μ_{f1}, μ_{f2}, μ_{f3}, μ_{f4}, μ_{f5}, μ_{f6}, y_3, z_3, N_3, M_{y_3}, M_{z_3}, A_3, ε_{C_3}, κ_{y_3} and κ_{z_3} respectively, where y_3 and z_3 are the centroidal axes of the beam cross-section ahead of the front (Fig. 3), N_3, M_{y_3}, M_{z_3} are the axial force and the bending moments, ε_{C_3}, κ_{y_3} and κ_{z_3} are the strain in the centre of the beam cross-section and the curvatures, respectively, in the x_3y_3 and x_3z_3 planes.

The strain energy release rate can be calculated by substituting of u_{01}^*, u_{02}^* and u_{03}^* in Eq. (1) (the integration in Eq. (1) should be carried-out by using the MatLab computer program).

3. Numerical example

Longitudinal fracture in the beam configuration shown in Fig. 4 is analyzed by applying the solution to the strain energy release rate derived in section 2 of the present paper. It is assumed that the beam exhibits smooth material inhomogeneity in width and height directions. The beam is subjected to four-point bending (the external loading consists of two vertical forces, F, applied at the beam end sections). The beam cross-section is a rectangle of width, b, and height, $2h$. A vertical notch of depth, h_2, is introduced in the beam mid-span in order to generate conditions for longitudinal fracture. It assumed that a longitudinal crack of length, $2a$, is located symmetrically with respect to the mid-span. The heights of the lower and upper crack arms are denoted by h_1 and h_2, respectively. It should be noted that the longitudinal crack is located in beam portion, B_1B_2, that is loaded in pure bending (Fig. 4). It is obvious that the upper crack arm is free of stresses (Fig. 4). Therefore,

$$u_{02}^* = 0 \tag{18}$$

It should be mentioned that the crack is located in beam portion, B_1B_2, that is loaded in pure bending. Due to symmetry, only half of the beam, $l_1 + l_2 \le x_4 \le 2(l_1 + l_2)$, is considered in the analysis (Fig. 4).

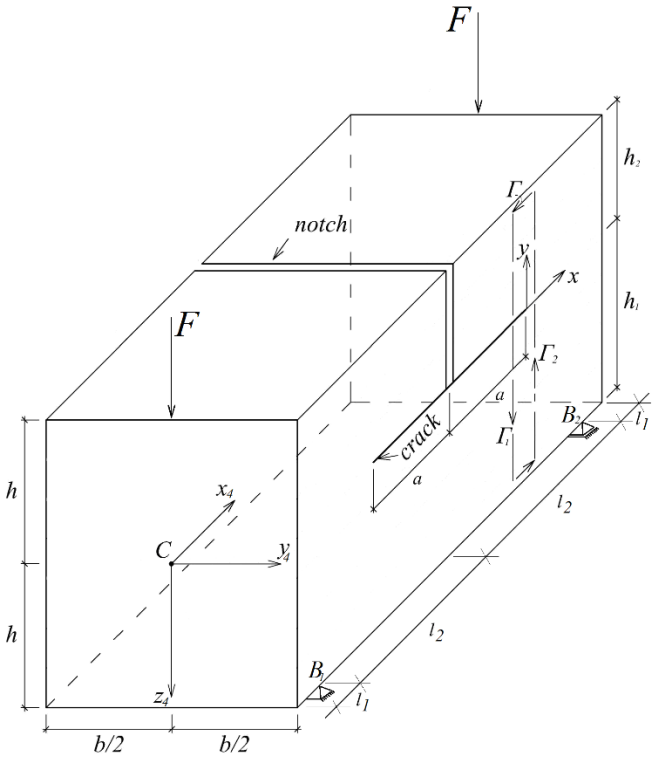

Fig. 4 Beam configuration with rectangular cross-section and a longitudinal crack located symmetrically with respect to the mid-span

The continuous variation of the modulus of elasticity in the beam cross-section is described by the following cosine law:

$$E = E_g \left[1 + m_1 \cos\left(\frac{\frac{b}{2} - y_4}{b} \frac{\pi}{2} \right) + m_2 \cos\left(\frac{h - z_4}{2h} \frac{\pi}{2} \right) \right] \tag{19}$$

where

$$-\frac{b}{2} \le y_4 \le \frac{b}{2} \tag{20}$$

$$-h \le z_4 \le h \tag{21}$$

In Eq. (19), y_4 and z_4 are the centroidal axes of the beam cross-section (Fig.4), E_g is the value of the modulus of elasticity in the upper left-hand vertex of the beam cross-section, m_1 and m_2 are material properties which govern the material inhomogeneity in width and height directions, respectively. It should be noted that trigonometric functions have been used for describing the material properties distribution in functionally graded materials (Arshad, Naeem and Sultana 2007).

Eq. (3) is used to obtain the complementary strain energy density in the cross-section of the lower crack arm behind the crack front. In order to express the distribution of the modulus of elasticity in the lower crack arm cross-section, Eq. (19) is re-written as

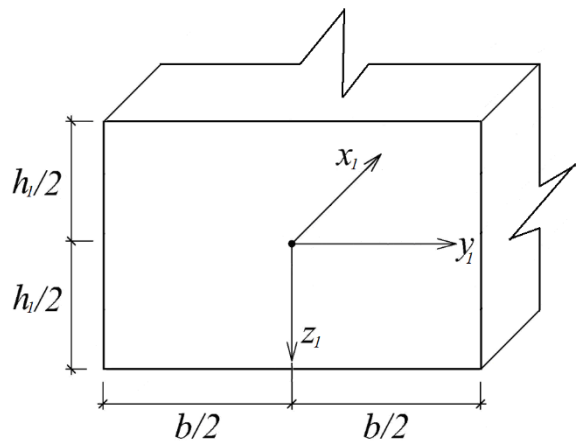

Fig. 5 Cross-section of the lower crack arm

$$E = E_g \left[1 + m_1 \cos\left(\frac{\frac{b}{2} - y_1}{b} \frac{\pi}{2} \right) + m_2 \cos\left(\frac{\frac{h_1}{2} - z_1}{2h} \frac{\pi}{2} \right) \right] \tag{22}$$

where

$$-\frac{b}{2} \le y_1 \le \frac{b}{2} \tag{23}$$

$$-\frac{h_1}{2} \le z_1 \le \frac{h_1}{2} \tag{24}$$

In Eq. (22), y_1 and z_1 are the centroidal axes of the lower crack arm cross-section (Fig. 5).

Further, by substituting of Eqs. (5) and (22) in Eqs. (9)-(17), one arrives at

$$\varepsilon_{C_1} = \frac{\mu_1}{E_g\left[\ 1 + m_1 0.707 + m_2 \cos\eta\ \right]} + \frac{\mu_1^{\frac{1}{n}}}{H^{\frac{1}{n}}} \tag{25}$$

$$\begin{aligned} &\kappa_{y_1} E_g \left(1 + m_1 0.707 + m_2 \cos\eta\right) + \\ &+ \varepsilon_{C_1} E_g m_1 0.353 \frac{\pi}{b} = \mu_2 + \\ &+ \frac{1}{H^{\frac{1}{n}}} \left(\begin{aligned} &E_g m_1 0.353 \frac{\pi}{b} \mu_1^{\frac{1}{n}} + \\ &+ E_g \left(1 + m_1 0.707 + m_2 \cos\eta\right) \frac{1}{n} \mu_1^{\frac{1-n}{n}} \mu_2 \end{aligned} \right) \end{aligned} \tag{26}$$

$$\begin{aligned} &\kappa_{z_1} E_g \left(1 + m_1 0.707 + m_2 \cos\eta\right) + \\ &+ \varepsilon_{C_1} E_g m_2 \frac{\pi}{4h} \sin\eta = \mu_3 + \end{aligned} \tag{27}$$

$$\begin{aligned} &2\kappa_{y_1} E_g m_1 0.353 \frac{\pi}{b} - \\ &\varepsilon_{C_1} E_g m_1 0.178 \frac{\pi^2}{b^2} = 2\mu_4 + \\ &+ \frac{1}{H^{\frac{1}{n}}} \Bigg\{ -E_g m_1 0.178 \frac{\pi^2}{b^2} \mu_1^{\frac{1}{n}} + \\ &+ E_g m_1 0.353 \frac{\pi}{b} \frac{1}{n} \mu_1^{\frac{1-n}{n}} \mu_2 + \\ &+ \Bigg[E_g m_1 0.353 \frac{\pi}{b} \frac{1}{n} \mu_1^{\frac{1-n}{n}} + \\ &+ E_g \left(1 + m_1 0.707 + m_2 \cos\eta\right) \frac{1-n}{n^2} \mu_1^{\frac{1-2n}{n}} \mu_2 \Bigg] \mu_2 + \\ &+ E_g \left(1 + m_1 0.707 + m_2 \cos\eta\right) \frac{2}{n} \mu_1^{\frac{1-n}{n}} \mu_4 \Bigg\} \end{aligned} \tag{28}$$

$$\begin{aligned} &\kappa_{y_1} E_g m_2 \frac{\pi}{4h} \sin\eta + \kappa_{z_1} E_g m_1 0.353 \frac{\pi}{b} = \mu_5 + \\ &+ \frac{1}{H^{\frac{1}{n}}} \Bigg[E_g m_1 0.353 \frac{\pi}{b} \frac{1}{n} \mu_1^{\frac{1-n}{n}} \mu_3 + \\ &+ \Bigg(E_g m_2 \frac{\pi}{4h} \sin\eta \frac{1}{n} \mu_1^{\frac{1-n}{n}} + \\ &+ E_g \left(1 + m_1 0.707 + m_2 \cos\eta \right) \frac{1-n}{n^2} \mu_1^{\frac{1-2n}{n}} \mu_3 \Bigg) \mu_2 + \\ &+ E_g \left(1 + m_1 0.707 + m_2 \cos\eta \right) \frac{1}{n} \mu_1^{\frac{1-n}{n}} \mu_5 \Bigg] \end{aligned} \tag{29}$$

$$\begin{aligned} &2\kappa_{z_1} E_g m_2 \frac{\pi}{4h} \sin\eta - \\ &\varepsilon_{C_1} E_g m_2 \frac{\pi^2}{16h^2} \cos\eta = 2\mu_6 + \\ &+ \frac{1}{H^{\frac{1}{n}}} \Bigg[-E_g m_2 \frac{\pi^2}{16h^2} \mu_1^{\frac{1}{n}} \cos\eta + \\ &+ E_g m_2 \frac{\pi}{4h} \frac{1}{n} \mu_1^{\frac{1-n}{n}} \mu_3 \sin\eta + \\ &+ \Bigg(E_g m_2 \frac{\pi}{4h} \frac{1}{n} \mu_1^{\frac{1-n}{n}} \sin\eta + \\ &+ E_g \left(1 + m_1 0.707 + m_2 \cos\eta\right) \frac{1-n}{n^2} \mu_1^{\frac{1-2n}{n}} \mu_3 \Bigg) \mu_3 + \\ &+ E_g \left(1 + m_1 0.707 + m_2 \cos\eta\right) \frac{2}{n} \mu_1^{\frac{1-n}{n}} \mu_6 \Bigg] \end{aligned} \tag{30}$$

$$N_{1`} = \mu_1 b h_1 + \mu_4 \frac{b^3 h_1}{12} + \mu_6 \frac{b h_1^3}{12} \tag{31}$$

$$M_{y_1} = \mu_3 \frac{b h_1^3}{12} \tag{32}$$

$$M_{z_1} = \mu_2 \frac{b^3 h_1}{12} \tag{33}$$

where $\eta = h_1 \pi / (8h)$ Figure 4 indicates that

$$N_1 = 0 \tag{34}$$

$$M_{y_1} = F l_1 \tag{35}$$

$$M_{z_1} = 0 \tag{36}$$

After solving of Eqs. (25)-(33) with respect to μ_1, μ_2, μ_3, μ_4, μ_5, μ_6, ε_{C_1}, κ_{y_1} and κ_{z_1} by using the MatLab computer program, the complementary strain energy density in the cross-section of the lower crack arm behind the crack front can be obtained by substituting of Eqs. (5) and (22) in Eq. (3).

In order to calculate the complementary strain energy density in the beam cross-section ahead of the crack front, first, μ_1, μ_2, μ_3, μ_4, μ_5, μ_6, ε_{C_1}, κ_{y_1} and κ_{z_1} and h_1 have to be replaced, respectively, with μ_{f1}, μ_{f2}, μ_{f3}, μ_{f4}, μ_{f5}, μ_{f6}, ε_{C_3}, κ_{y_3} and κ_{z_3} and $2h$ in Eqs. (25)-(33). Then, after solving Eqs. (25)-(33) by the MatLab computer program, the normal stress, σ_f, can be determined by Eq. (5) and substituted in Eq. (3) to obtain u_{03}^*.

After replacing of b_s with b and substituting of u_{01}^*, u_{02}^* and u_{03}^* in Eq. (1), the strain energy release rate, calculated by the MatLab computer program, is doubled in view of the symmetry (Fig. 4).

The solution to the strain energy release rate is verified by applying the *J*-integral approach (Broek 1986) for analyzing the longitudinal crack in the beam shown in Fig. 4. The *J*-integral is solved along the integration contour, Γ, shown by dashed line in Fig. 4. Since the upper crack arm is free of stresses, the *J*-integral value is zero in the upper crack arm. Therefore, the *J*-integral solution is written as

$$J = 2(J_{\Gamma_1} + J_{\Gamma_2}) \tag{37}$$

In Eq. (37), the *J*-integral values in segments, Γ_1 and Γ_2, of the integration contour are denoted by J_{Γ_1} and J_{Γ_2}, respectively. The segments, Γ_1 and Γ_2, coincide, respectively, with the cross-sections of the lower crack arm and the beam ahead of the crack front (Fig. 4). It should be noted that the term in brackets in Eq. (37) is doubled in view of symmetry (Fig. 4).

The *J*-integral in segment, Γ_1, of the integration contour is written as

$$J_{\Gamma_1} = \int_{\Gamma_1} \left[u_{01} \cos\alpha_{\Gamma_1} - \left(p_{x_{\Gamma_1}} \frac{\partial u}{\partial x_{\Gamma_1}} + p_{y_{\Gamma_1}} \frac{\partial v}{\partial x_{\Gamma_1}} \right) \right] ds_{\Gamma_1} \tag{38}$$

where u_{01} is the strain energy density in the cross-section of lower crack arm behind the crack front, α_{Γ_1} is the angle between the outwards normal vector to the contour of integration and the crack direction, $p_{x_{\Gamma_1}}$ and $p_{y_{\Gamma_1}}$ are the components of the stress vector, u and v are the components of the displacement vector with respect to the coordinate system xy, and $d_{s_{\Gamma_1}}$ is a differential element along the contour of integration.

The components of Eq. (38) are expressed as

$$p_{x_{\Gamma_1}} = -\sigma \tag{39}$$

$$p_{y_{\Gamma_1}} = 0 \tag{40}$$

$$ds_{\Gamma_1} = dz_1 \tag{41}$$

$$\frac{\partial u}{\partial x_{\Gamma_1}} = \varepsilon = \frac{\sigma}{E} + \left(\frac{\sigma}{H}\right)^{\frac{1}{n}} \tag{42}$$

$$\cos\alpha_{\Gamma_1} = -1 \tag{43}$$

In Eqs. (39) and (42), the normal stress, σ, is determined by Eq. (5). The coordinate, z_1, in Eq. (41) varies in the interval [$-h_1/2$; $h_1/2$]. The strain energy density in the cross-section of lower crack arm is calculated by the following formula (Rizov 2017a)

$$u_{01} = \frac{\sigma^2}{2E} + \frac{\sigma^{\frac{1+n}{n}}}{(1+n)H^{\frac{1}{n}}} \tag{44}$$

where σ is obtained by Eq. (5).

The *J*-integral in segment, Γ_2, is expressed as

$$J_{\Gamma_2} = \int_{\Gamma_2} \left[u_{02} \cos\alpha_{\Gamma_2} - \left(p_{x_{\Gamma_2}} \frac{\partial u}{\partial x_{\Gamma_2}} + p_{y_{\Gamma_2}} \frac{\partial v}{\partial x_{\Gamma_2}} \right) \right] ds_{\Gamma_2} \tag{45}$$

The components of Eq. (45) are determined as

$$p_{x_{\Gamma_2}} = \sigma_f \tag{46}$$

$$p_{y_{\Gamma_2}} = 0 \tag{47}$$

$$ds_{\Gamma_2} = -dz_3 \tag{48}$$

$$\cos\alpha_{\Gamma_2} = 1 \tag{49}$$

$$\frac{\partial u}{\partial x_{\Gamma_2}} = \frac{\sigma_f}{E} + \left(\frac{\sigma_f}{H}\right)^{\frac{1}{n}} \tag{50}$$

$$u_{01} = \frac{\sigma_f^2}{2E} + \frac{\sigma_f^{\frac{1+n}{n}}}{(1+n)H^{\frac{1}{n}}} \tag{51}$$

where the coordinate, z_3, varies in the interval [$-h$;h]. The stress, σ_f, in Eqs. (46), (50) and (51) is calculated by Eq. (5).

The average value of the *J*-integral along the crack front is written as

$$J_{av} = \frac{1}{b} \int_{-\frac{b}{2}}^{\frac{b}{2}} J\, dy_1 \tag{52}$$

By substituting of Eqs. (37), (38) and (45) in Eq. (52), one arrives at

$$J_{av} = \frac{2}{b}\int_{-\frac{b}{2}}^{\frac{b}{2}}\int_{-\frac{h_1}{2}}^{\frac{h_1}{2}}\left[\begin{array}{l} u_{01}\cos\alpha_{\Gamma_1} - \\ \left(p_{x_{\Gamma_1}}\dfrac{\partial u}{\partial x_{\Gamma_1}} + p_{x_{\Gamma_1}}\dfrac{\partial v}{\partial x_{\Gamma_1}}\right)\end{array}\right]dy_1 ds_{\Gamma_1} + \\ + \frac{2}{b}\int_{-\frac{b}{2}}^{\frac{b}{2}}\int_{-h}^{h}\left[\begin{array}{l} u_{02}\cos\alpha_{\Gamma_2} - \\ \left(p_{x_{\Gamma_2}}\dfrac{\partial u}{\partial x_{\Gamma_2}} + p_{y_{\Gamma_2}}\dfrac{\partial v}{\partial x_{\Gamma_2}}\right)\end{array}\right]dy_1 ds_{\Gamma_2} \tag{53}$$

The MatLab computer program is used to carry-out the integration in Eq. (53). The *J*-integral values obtained by Eq. (53) are exact matches of the strain energy release rates calculated by Eq. (1). This fact verifies the fracture analysis developed in the present paper. It should be noted that the fracture is analyzed also by keeping more than six members in the series of Maclaurin Eq. (4). The results are very close to these obtained by keeping six members (the difference is less than 2 %).

Influences of material inhomogeneity along the width and height of the beam, the crack location along the beam height and the non-linear mechanical behaviour of the inhomogeneous material on the longitudinal fracture in the beam configuration shown in Fig. 4 are investigated. For this purpose, calculations of the strain energy release rate are performed by Eq. (1). The results obtained are presented in non-dimension form by using the formula $G_N = G/(E_g b)$. It is assumed that b = 0.010 m, h = 0.0015 m, l_1 = 0.010 m, l_2 = 0.060 m, a = 0. 0050 m and F = 30 N. Also, it is assumed that E_g = 110 GPa. The properties, m_1 and m_2, which characterize the material inhomogeneity along the width and height of the beam (refer to Eq. (22)) are varied in the analysis in order to evaluate their effect on the longitudinal fracture behavior. The crack location along the beam height is characterized by $h_2/2h$ ratio.

The strain energy release rate in non-dimensional form is presented as a function of m_1 in Fig. 6 for three $h_2/2h$ ratios at m_2 = 0.6, H/E_g = 0.7 and n = 0.8. The curves in Fig. 6 indicate that the strain energy release rate decreases with increasing of m_1. This finding is attributed to the increase of the beam stiffness. One can observe also in Fig. 6 that the strain energy release rate decreases with increasing of $h_2/2h$ ratio. This behavior is due to the increase of the height of the lower crack arm.

The finite element method is used also for verification of the solution to the strain energy release rate. For this purpose, first, a formula for the strain energy release rate is derived by considering the balance of the energy for the longitudinal crack in the beam configuration shown in Fig. 4. In order to determine the strain energy release rate, a small increase, δa, of the crack length is assumed. The energy balance is expressed as

$$F\delta w = \frac{\Delta U}{\Delta a}\delta a + Gb\delta a \tag{54}$$

where w is the vertical displacement of the application point of the external force, F, ΔU is the change of the strain

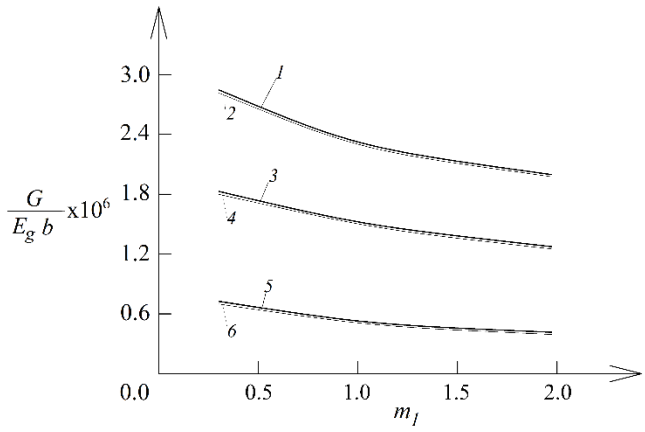

Fig. 6 The strain energy release rate in non-dimensional form presented as a function of m_1 at (curve 1) $h_1/2h$ = 0.30 analytical solution, (curve 2) $h_1/2h$ = 0.30 Finite Element (FE) analysis, (curve 3) $h_2/2h$ = 0.50 analytical solution, (curve 4) $h_2/2h$ = 0.50 FE analysis, (curve 5) $h_2/2h$ = 0.70 analytical solution and (curve 6) $h_2/2h$ = 0.70 FE analysis

energy cumulated in the beam. Form Eq. (54), one obtains the following expression for the strain energy release rate where Δw is the change of the vertical displacement due to

$$G = 2\left(\frac{F}{b}\frac{\Delta w}{\Delta a} - \frac{1}{b}\frac{\Delta U}{\Delta a}\right) \tag{55}$$

crack increase. It should be noted that the term in brackets in Eq. (55) is doubled in view of the symmetry (Fig. 4). In order to calculate the strain energy release rate by Eq. (55), a three-dimensional finite element model of the beam is developed by using the ANSYS computer program. Due to the symmetry (Fig. 4), only half of the beam in longitudinal direction, $0 \le x_4 \le l_1 + l_2$, is modeled by the finite element method. In order to simulate the symmetry, the following boundary conditions are used: the longitudinal components (along x_4-axis) of the displacements of the nodes in the cross-section of the lower crack arm in the beam mid-span, $x_4 = l_1 + l_2$, are set to zero. The external loading is presented as a uniformly distributed load across the beam width of intensity, F/b, applied at the end section, $x_4 = 0$, of the beam. Solid finite elements SOLID45 are used to mesh the model. The finite element SOLID45 is defined by eight nodal points (one in each vertex). Each nodal point has three degrees of freedom (translations in x, y and z nodal directions). The finite element mesh is refined in the vicinity of the crack front. The total number of finite elements used in the simulations is 42600. It should be mentioned that this number of elements is chosen after performing a mesh sensitivity study to ensure that the mesh is fine enough. A typical finite element mesh is shown in Fig. 7. The smallest and largest element sizes used are 0.0002 m and 0.0015 m, respectively. The Poisson's ratio is set to 0.3 in the finite element model.

The distribution of the modulus of elasticity of the inhomogeneous material in the beam cross-section is treated

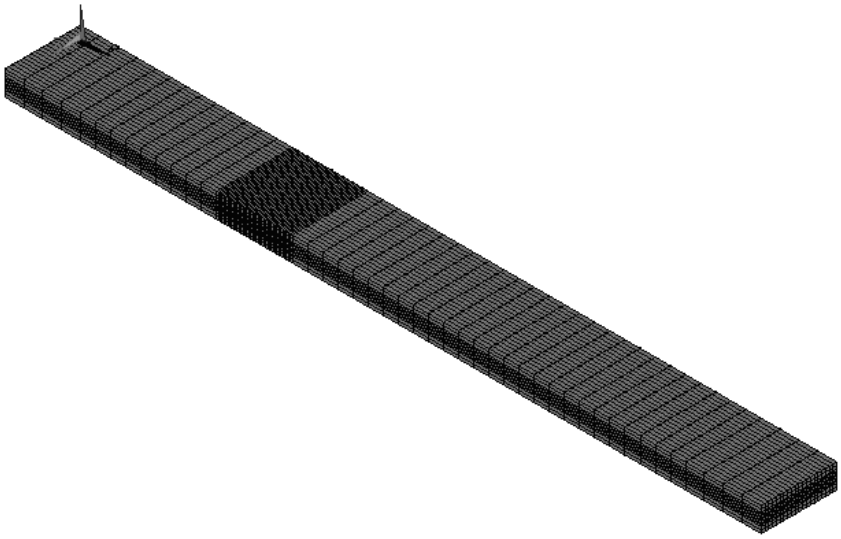

Fig. 7 Three-dimensional mesh used in the finite element simulations

Table 1 Convergence of the strain energy release rate, G_N, as a function of Δa towards the analytical solution, $G_N^a = 2.657$

Δa, mm	G_N
0.0004	2.586
0.0002	2.650
0.0001	2.650

in the finite element model in the following way. The beam cross-section in the finite element model is divided into rectangles. The value of the modulus of elasticity calculated by Eq. (22) for the coordinates of the centre of a given rectangle is assigned to the finite elements located in this rectangle. A multi-linear isotropic hardening material model is used in the finite element simulations. According to this material model, the Ramberg-Osgood stress-strain curve is defined point by point. For this purpose, Eq. (2) and the modulus of elasticity calculated by Eq. (22) for the centre of a given rectangle are used. The multi-linear stress-strain curve constructed in this manner is assigned to finite elements located in the corresponding rectangle of the beam cross-section. In this way, a stepwise distribution of the material properties in the cross-section of the inhomogeneous beam is realized in the finite element analysis since the finite elements located in individual rectangles have one and the same properties (modulus of elasticity and stress-strain curve). It should be noted that the dimensions of the finite element model and the values of material properties are identical with these used in the analytical solution.

Application of Eq. (55) for the strain energy release rate necessitates calculation of the difference, ΔU, between the strain energy cumulated in the beam before and after increase of the crack length with Δa by using the finite element model. It is necessary to calculate also the difference, Δw, between the vertical displacement of the application point of the external force before and after increase of the crack length. In the finite element analysis, a crack increase of Δa = 0.0002 m is used. This value of the crack increase is chosen after performing a sensitivity study to ensure that further decreasing of Δa does not affect the results of the analysis. The results of the sensitivity study are illustrated in Table 1 where the convergence of the strain energy release rates as a function of Δa towards the analytical solution is presented. One can observe in Table 1 that the strain energy release rate does not change when Δa decreases from 0.0002 m to 0.0001 mm. Therefore, Δa = 0.0002 m is used in the analysis. The enlarged near crack tip mesh is shown in Fig. 8. The strain energy release rate obtained by the finite element model via Eq. (55) is presented as a function of m_1 in Fig. 6.

One can observe that the results obtained by the solution to the strain energy release rate derived in section 2 of the present paper are in a very good agreement with these obtained by the finite element simulations (Fig. 6).

In order to analyze the effect of m_2 on the longitudinal fracture behavior, the strain energy release rate obtained by Eq. (1) is presented in non-dimensional form as a function of m_2 in Fig. 9 at $h_2/2h$ = 0.3 and m_1 = 0.5. It can be observed in Fig. 9 that the strain energy release rate decreases with increasing of m_2. The influence of the non-linear mechanical behavior of the inhomogeneous material on the longitudinal fracture is evaluated too. For this purpose, the strain energy release rate obtained assuming linear-elastic behavior of the inhomogeneous material is presented in non-dimensional form as a function of m_2 in Fig. 9 for comparison with the non-linear solution. It should be noted that the linear-elastic solution to the strain energy release rate is derived by substituting of H → ∞ in the non-linear solution Eq. (1) (this is due to the fact that at H → ∞ the Ramberg-Osgood stress-strain Eq. (2) transforms into the Hooke's law assuming that E is the modulus of elasticity of the inhomogeneous material). One can observe that the non-linear mechanical behavior of the material leads to increase of the strain energy release rate (Fig. 9) which is

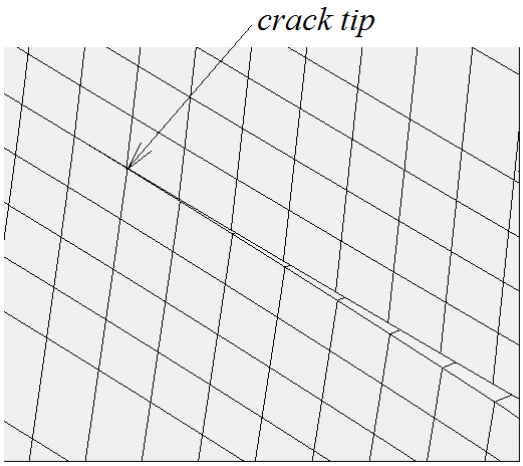

Fig. 8 Enlarged near crack tip mesh in deformed state at the lateral surface of the beam

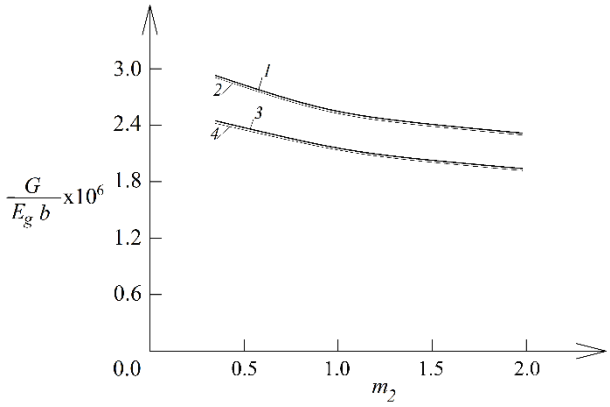

Fig. 9 The strain energy release rate in non-dimensional form presented as a function of m_2 at (curve 1) non-linear elastic behavior of the material (analytical solution), (curve 2) non-linear elastic behavior of the material (FE analysis), (curve 3) linear-elastic behavior of the material (analytical solution) and (curve 4) linear-elastic behavior of the material (FE analysis)

due to decrease of the beam stiffness. Results obtained by the finite element model are also presented in Fig. 9.

The curves in Fig. 9 demonstrate a very good agreement between the solution derived in section 2 of the present paper and the finite element analysis.

4. Conclusions

A solution to the strain energy release rate for longitudinal cracks in beam configurations which exhibit smooth material inhomogeneity along the width as well as along the height of the beam cross-section is derived assuming non-linear mechanical behavior of the material. Besides, it is assumed that the stiffness properties are constant along the beam axis. The beams which are under combination of axial force and bending moments may have arbitrary cross-section. The Ramberg-Osgood equation is applied for treating the material non-linearity. The solution derived holds for longitudinal cracks located arbitrary along the height of the beam cross-section. Besides, the modulus of elasticity may be distributed arbitrary in the beam cross-section. The solution is used for analyzing the strain energy release rate in a beam configuration that contains a longitudinal crack located symmetrically with respect to the mid-span. The continuous variation of the modulus of elasticity in the beam cross-section is described by a cosine law. The fracture is studied also by the *J*-integral for verification. The finite element method is also applied for verification of the solution to the strain energy release rate. Effects of material inhomogeneity in width and height direction of the cross-section, material non-linearity and crack location along the beam height are investigated. The analysis reveals that the strain energy release rate decreases with increasing of m_1 and m_2 (m_1 and m_2) are material properties which control the material inhomogeneity in width and height directions, respectively). It is found also that the strain energy release rate decreases with increasing of the height of the lower crack arm. A comparison with the strain energy release rate derived assuming linear-elastic mechanical behavior of the inhomogeneous material is performed. It is found that the material non-linearity leads to increase of the strain energy release rate.

References

Arshad, S.H., Naeem, M.N. and Sultana, N. (2007), "Frequency analysis of functionally graded material cylindrical shells with various volume fraction laws", *Proceedings of the Institution of Mechanical Engineers, Part C J. Mech. Eng. Sci.,* **221**(12), 1483-1495. https://doi.org/10.1243/09544062JMES738.

Bohidar, S.K., Sharma, R. and Mishra, P.R. (2014), "Functionally graded materials: A critical review", *J. Res.,* **1**(7), 289-301.

Broek, D. (1986), *Elementary Engineering Fracture Mechanics*, Springer, Germany.

Carpinteri, A., Paggi, M. and Pugno, N. (2006), "An analytical approach for fracture and fatigue in functionally graded materials", *J. Fracture*, **141**(2), 535-547. https://doi.org/10.1007/s10704-006-9012-y.

Wei, D., Liu, Y. and Xiang, Z. (2012), "An analytical method for free vibration analysis of functionally graded beams with edge cracks", *J. Sound Vib.*, **331**(2), 1686-1700. https://doi.org/10.1016/j.jsv.2011.11.020.

Dowling, N. (2007), *Mechanical Behavior of Materials*, Pearson, USA.

Gasik, M.M. (2010), "Functionally graded materials: Bulk processing techniques", *J. Mater. Product. Technol.*, **39**(1-2), 20-29. https://doi.org/10.1504/IJMPT.2010.034257.

Hirai, T. and Chen, L. (1999), "Recent and prospective development of functionally graded materials in Japan", *Mater Sci. Forum,* **308-311**(4), 509-514. https://doi.org/10.4028/www.scientific.net/MSF.308-311.509.

Koizumi, M. (1993), "The concept of FGM Ceramic Trans", *Functionally Gradient Materials*, **34**(1), 3-10.

Markworth, A.J., Ramesh, K.S. and Parks, Jr.W.P. (1995), "Review: Modeling studies applied to functionally graded materials", *J. Mater. Sci.*, **30**(3), 2183-2193. https://doi.org/10.1007/BF01184560.

Mortensen, A. and Suresh, S. (1995), "Functionally graded metals and metal-ceramic composites: Part 1 Processing", *Int. Mater. Rev.*, **40**(6), 239-265. https://doi.org/10.1179/imr.1995.40.6.239.

Mousavi, S.M. and Paavola, I. (2013), "Analysis of functionally graded magneto-electro-elastic layer with multiple cracks",

Theoerital Appl. Fracture Mech., **66**(1), 1-8. https://doi.org/10.1016/j.tafmec.2013.11.007.

Nemat-Allal, M.M., Ata, M.H., Bayoumi, M.R. and Khair-Eldeen, W. (2011), "Powder metallurgical fabrication and microstructural investigations of Aluminum/Steel functionally graded material", *Mater. Sci. Appl.*, **2**(5), 1708-1718.

Neubrand, A. and Rödel, J. (1997), "Gradient materials: An overview of a novel concept", *Zeit. f. Met.*, **88**(4), 358-371.

Rekik, M., El-Borgi, S. and Ounaies, Z. (2014), "An axisymmetric problem of an embedded mixed-mode crack in a functionally graded magnetoelectroelastic infinite medium", *Appl. Math. Modell.*, **38**(4), 1193-1210. https://doi.org/10.1016/j.ijsolstr.2011.12.002.

Rizov, V. (2017a), "Delamination analysis of a layered elastic-plastic beam", *J. Struct. Integrity*, **8**(4), 516-529.

Rizov, V. (2017b), "An analytical solution to the strain energy release rate of a crack in functionally graded beams", *Europ. J. Mech. A/solids*, **65**(2), 301-312. https://doi.org/10.1016/j.euromechsol.2017.04.005.

Rizov, V. (2017c), "Fracture analysis of functionally graded beams with considering material non-linearity", *Struct. Eng. Mech.*, **64**(4), 487-494. http://dx.doi.org/10.12989/sem.2017.64.4.487.

Rizov, V. (2017d), "Analytical study of elastic-plastic longitudinal fracture in a functionally graded beam", *Strength, Fracture Complexity*, **10**(1), 11-22. https://doi.org/10.3233/SFC-170197.

Rizov, V.I. (2018a), "Lengthwise fracture analyses of functionally graded beams by the Ramberg-Osgood equation", *Eng. Rev.,* **38**(2), 309-320. https://hrcak.srce.hr/201161.

Rizov, V.I. (2018b), "Delamination in multi-layered functionally graded beams – an analytical study by using the Ramberg-Osgood equation", *Struct. Integrity Life*, **18**(1), 70-76.

Rizov, V.I. (2018c), "Analytical study of delamination in multilayered two-dimensional functionally graded non-linear elastic beams," *J. Mech.*, **34**(4), 496-504. https://doi.org/10.1017/jmech.2017.104.

Suresh, S. and Mortensen, A. (1998), *Fundamentals of Functionally Graded Materials*, IOM Communications Ltd., London, United Kingdom.

Wang, B.L. and Noda, N. (2001), "Thermally induced fracture of a smart functionally graded composite structure", *Theoretial Appl. Fracture Mech.*, **35**(1), 93-109. https://doi.org/10.1016/S0167-8442(00)00052-5.

PL